



**HAL**  
open science

## Contribution of moderate climate events to atoll island building (Fakarava Atoll, French Polynesia)

Virginie Duvat, Valentin Pillet, Natacha Volto, Heitea Terorotua, Victoire Laurent

► **To cite this version:**

Virginie Duvat, Valentin Pillet, Natacha Volto, Heitea Terorotua, Victoire Laurent. Contribution of moderate climate events to atoll island building (Fakarava Atoll, French Polynesia). *Geomorphology*, 2020, 354, pp.107057. 10.1016/j.geomorph.2020.107057 . hal-02502319

**HAL Id: hal-02502319**

**<https://hal.science/hal-02502319v1>**

Submitted on 17 Sep 2024

**HAL** is a multi-disciplinary open access archive for the deposit and dissemination of scientific research documents, whether they are published or not. The documents may come from teaching and research institutions in France or abroad, or from public or private research centers.

L'archive ouverte pluridisciplinaire **HAL**, est destinée au dépôt et à la diffusion de documents scientifiques de niveau recherche, publiés ou non, émanant des établissements d'enseignement et de recherche français ou étrangers, des laboratoires publics ou privés.

1 **Contribution of moderate climate events**  
2 **to atoll island building (Fakarava, French Polynesia)**

3  
4 **1. Introduction**

5 Extreme climate events, including storm-related (i.e. tropical cyclones and distant-source  
6 swells) and El Niño- and La Niña-related, are widely acknowledged to play a major role in  
7 atoll island change through a complex combination of erosional and accretional processes  
8 (Nurse et al., 2014). The effects of tropical cyclones on atoll islands have been extensively  
9 investigated since the 1960s, and their contrasting, i.e. both destructive and constructional,  
10 impacts highlighted at different spatial-temporal scales (Stoddart, 1969, 1971; Maragos et al.,  
11 1973; Baines et al., 1974; Baines and McLean, 1976; Woodroffe, 1983; Scoffin, 1993; Le  
12 Cozannet et al., 2013; Ford and Kench, 2014, 2016; Duvat and Pillet, 2017; Duvat et al.,  
13 2017a, 2017b). In addition, over the past decade a growing number of studies have reported  
14 the impacts of distant-source swells on Pacific and Indian Oceans' atoll islands (Hoeke et al.,  
15 2013; Smithers and Hoeke, 2014; Aslam and Kench, 2018; Wadey et al., 2018; Canavesio,  
16 2019). These studies have shown that such events, which had until recently remained poorly  
17 understood, also contribute significantly to atoll island change, in particular through  
18 overwash-driven processes that cause island erosion and/or building, depending on the  
19 context. Together, these studies have underscored that the response of atoll islands to cyclonic  
20 and distant-source swells is influenced by human interferences with natural processes,  
21 including in particular the removal of the coastal vegetation or the replacement of native  
22 species by introduced species (Stoddart, 1963, 1965; Duvat et al., 2017a), the obstruction or  
23 reduction in width of inter-islet channels as a result of land reclamation (Canavesio, 2019),  
24 and shoreline hardening (Smithers and Hoeke, 2014). Although they have been less  
25 investigated, the effects of El Niño and La Niña phases on alongshore sediment transport, and

26 thereby on shoreline change, have been studied in Kiribati, where Rankey (2011) reported  
27 beach migration. Moreover, El Niño events play a major role in the occurrence of tropical  
28 cyclones in some ocean regions (e.g. Tuamotu Archipelago, Central Pacific) that are located  
29 outside the cyclone belt and are only liable to experience tropical cyclones under El Niño  
30 conditions (Larrue and Chirron, 2010). Additionally, some studies have emphasised the major  
31 role of tsunami in atoll island building, for example in the Maldives, following the 2004  
32 Sumatra tsunami (Kench et al., 2006). Generally, it can be noted that intense events, either  
33 climate- or tectonic-related, have so far been the main focus of atoll geomorphic studies. The  
34 influence of moderate climate events, such as tropical lows that do not reach the cyclone stage  
35 and low-magnitude distant-source swells, has to date been overlooked. However, because  
36 they are much more frequent than extreme climate events, these events can be assumed to  
37 contribute significantly to atoll island change, especially in regions where intense climate  
38 events are uncommon.

39 This article addresses this research gap by focusing on a moderate climate event, i.e. tropical  
40 low 13F, which affected the northern part of Fakarava Atoll, Tuamotu Archipelago, in  
41 February 2017. Based on multi-date image analysis and field observations which were  
42 conducted before, immediately after and one year after the event, it demonstrates that  
43 moderate climate events significantly contribute to atoll island change. This article especially  
44 underscores their constructional effects and the interferences between the physical processes  
45 operating during such events and human activities. It then discusses the implications of  
46 findings for future research and coastal risk reduction on atoll islands.

47

## 48 **2. Context of the study**

### 49 **2.1. Study area**

50 The Tuamotu Archipelago is one of the five archipelagos composing French Polynesia (Fig.  
51 1) and the largest group of atolls (77) in the world. It is composed of two chains of atolls and  
52 stretches >1,500 km from northwest to southeast, extending from 14°21'S to 23°22'S and  
53 from 134°28'W to 148°43'W. Fakarava Atoll is located in the northwestern part of the  
54 Tuamotu Archipelago at 16°18'S and 145°36'W (Fig. 1), and is the second largest atoll  
55 (1.246 km<sup>2</sup>) of this archipelago after Rangiroa (1.762 km<sup>2</sup>). It exhibits a rectangular shape,  
56 measures approximately 54.9 km long from northwest to southeast, and has a maximum width  
57 of 24.9 km (Fig. 2a). Fakarava is an open atoll having two passes connecting the open ocean  
58 to the lagoon at its northern (Garuae Pass) and southern (Temakohua Pass) extremities. Its  
59 lagoon is one of the deepest of the Tuamotu Archipelago, with a maximum depth of  
60 approximately 60 m (Rougerie, 1994). The total land area of the islands that have formed on  
61 the atoll rim is approximately 27 km<sup>2</sup>. The study area is located on the northern part of the  
62 atoll rim, and is composed of five islands stretching >14 km between the Garuae Pass, in the  
63 central north, and the southern end of the main village, Rotoava, located in the north-eastern  
64 angle of the atoll (Fig. 2b). These islands are 180 to 380 m wide and perched on a  
65 conglomerate platform which extends by 50 to 100 m seaward from the base of the beach. On  
66 their north-facing ocean coast, they exhibit a more or less dense vegetation belt composed of  
67 native species (*Pemphis acidula*, *Suriana maritima*, *Scaevola taccada*, *Guettarda speciosa*,  
68 *Tournefortia argentea*). The population of Fakarava counted 674 inhabitants in 2017, most of  
69 which live in the village (ISPF, 2017).

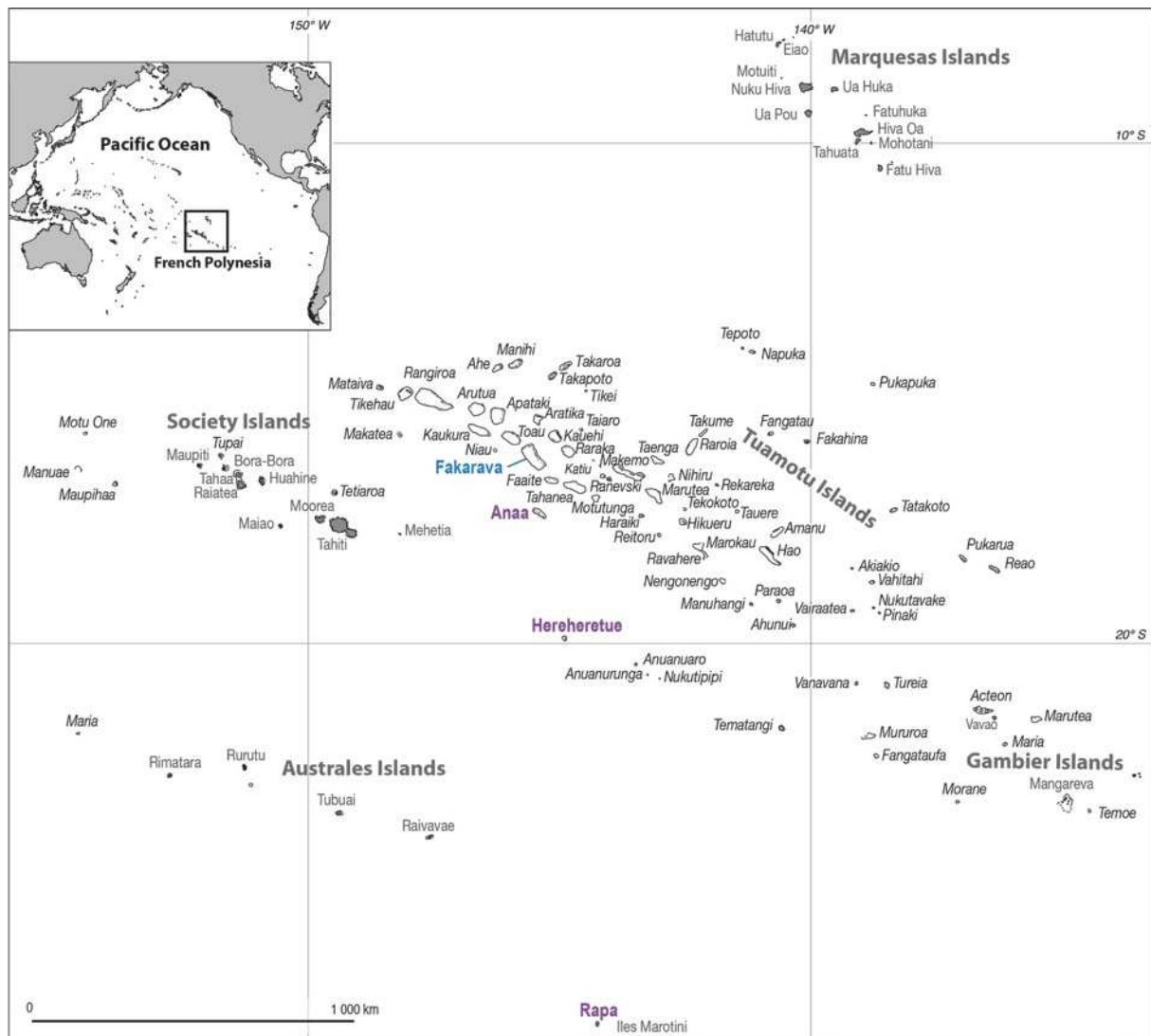
70 The climate regime of the study area is controlled by the combined influence of the trade  
71 winds from the northeast to southeast directions, and of tropical and extra-tropical storms  
72 (Andrefouët et al., 2012). In the Austral Summer (November-March), trade winds are weak  
73 and generate moderate waves that can be disturbed by storm waves originating either from  
74 tropical cyclones (especially during El Niño phases), or from distant storms forming in

75 northern latitudes. However, like other Tuamotu atolls, Fakarava is rarely affected by tropical  
76 cyclones, the return period of which is ~39 years (Larrue and Chiron, 2010). The last tropical  
77 cyclone that affected Fakarava was Orama (category 3) in February 1983 (Laurent and  
78 Varney, 2014). During the Austral Summer, Fakarava is relatively protected from northern  
79 distant-source waves by northern atolls due to the atoll ‘shadow effect’ (Andrefouët et al.,  
80 2012). In the Austral Winter (April-October), the combination of stronger trade winds  
81 (northeast-southeast, clockwise) and stronger distant-source southern swells generate more  
82 energetic conditions in the western Tuamotu region. During this season, Fakarava is highly  
83 exposed to the distant-source swells originating from the south and southwest, as a result of  
84 its location at the western border of the Tuamotu Archipelago.

85 In the western Tuamotu atolls, the mean tidal range is approximately 0.5 m and reaches an  
86 average of 0.65 m at spring tide (Pirazzoli and Montaggioni, 1986). Based on the  
87 reconstruction of sea levels in the Pacific Island Region over a 60-year time period (1950–  
88 2009), Becker et al.

89 (2012) estimated absolute sea-level rise in the northern Tuamotu region to be  $2.5 \pm 0.5$  mm/y.  
90 This rate is higher than the global mean sea-level rise for the twentieth century, which was  
91 estimated to be ~1.8 mm/y by Church and White (2011) and  $1.2 \pm 0.2$  mm/y by Hay et al.  
92 (2015). This value is comparable to the absolute sea-level rise estimated for the Marshall  
93 ( $1.4 \pm 0.6$  mm/y at Majuro) and Gilbert Islands ( $2.2 \pm 0.6$  mm/y at Tarawa), but smaller than the  
94 maximal rate of  $4.7 \pm 0.7$  mm/y obtained for Funafuti Atoll in Tuvalu (Becker et al., 2012).

95



96

97 Figure 1. Location map of the study area.

98 Fakarava Atoll is shown in blue. Other locations mentioned in the text are shown in purple.

99

100 **2.2. Meteorological event of February 2017**

101 From 13 to 20 February 2017, a tropical low developed within the South Pacific Convergence  
 102 Zone, which generated strong winds and swells across the northern Tuamotu atolls. Named  
 103 13F by the Fiji Meteorological Service on 16 February, it moved on an axis stretching from  
 104 the Society Islands to the Centre Tuamotu and Australes Islands. On 16 February at 2 pm,  
 105 French Polynesia time, the tropical low was centred 60 km to the west of Hereheretue, with  
 106 mean sea level pressure of 999.8 hPa measured on Anaa. It generated northwesterly

107 maximum sustained 10-min winds of 74 km/h, with the highest gusts reaching 106 km/h on  
108 Hao. These strong winds generated strong swells, with wave height reaching between 4 to  
109 4.9 m at Fakarava and up to 6.1 m between Anaa and Hereheretue. Due to the northwesterly  
110 origin of the swells, this event mainly impacted the northwestern and northern sides of the  
111 atoll, including the village of Rotoava. The inhabitants of the village estimated that wave  
112 height reached up to 4 m on the northeastern ocean coast of the main island (Terorotua, 2017).  
113 On Fakarava, the winds and swells caused the cancellation of all flights connecting the atoll to  
114 other destinations from 15 February to 19 February. On 17 February, tropical low 13F moved  
115 to the south-east of Tahiti, with estimated central pressure of 992 hPa, then to the northeast of  
116 Rapa on 18, and eventually left French Polynesia on 19 February. From Gumbel distribution,  
117 the return period of such an event is two years from mean sea level pressure (992hPa) and  
118 three years from maximum significant wave height (6.1 m).  
119 Compared to the most intense tropical cyclones that have affected the northwestern Tuamotu  
120 atolls over the past century – that is, tropical cyclones Orama and Veena, in February and  
121 April 1983, respectively – tropical low 13F can be considered a moderate event. For example,  
122 tropical cyclone Orama, which severely affected the northwestern atolls of the Tuamotu chain  
123 including Fakarava Atoll, exhibited a minimum sea level pressure of 925 hPa, sustained  
124 winds of 185 km/h and a maximum wave height of ~9 m on the most exposed (i.e. southern)  
125 coast of nearby Rangiroa Atoll (Duvat et al., 2018).

126

### 127 **3. Materials and Methods**

#### 128 **3.1. Fieldwork**

129 Two field trips allowed to document the morphological impacts of tropical low 13F. The first  
130 one took place in February 2017, including immediately before and immediately after the  
131 event, as some of the authors were conducting fieldwork on the atoll when the event occurred.

132 This allowed to make a qualitative assessment of the erosional and accretional geomorphic  
133 features generated by this event along 14 km of ocean-facing shoreline between Garuae Pass  
134 and the village (see locations on Fig. 2b). This first field trip allowed to directly observe and  
135 thus precisely attribute impacts to tropical low 13F, and to comprehend the respective  
136 importance of erosional and accretional features in the study area. Additionally, field  
137 observations were used to validate the mapping of sediment deposits derived from satellite  
138 image analysis (see section 3.2). Observations were made in the intertidal zone, i.e. on the  
139 ocean-side reef flat, in hoa (i.e. inter-island channels), in the coastal zone on both ocean and  
140 lagoon shores, and in inland areas. This first field trip also allowed to conduct interviews with  
141 both local residents living in the impacted area and diving instructors who made direct  
142 observations of impacts on the northern outer slopes of the atoll a few days after the event.  
143 These interviews allowed to collect information on wave height at the coast, morphological  
144 impacts inland (e.g. sediment deposition in properties) and the mechanical destruction of  
145 corals on the outer slopes.

146 The second field trip was conducted from 3 to 10 March 2018, that is, approximately one year  
147 after the event, in order to study shoreline readjustment and reef-to-shore sediment transfer  
148 resulting from the dismantling of the accretional features that had formed in the intertidal  
149 zone during the event. During this field trip, we took Unmanned Aerial Vehicle (UAV)  
150 images in areas exhibiting remarkable accretional features, such as storm ramparts (see  
151 location in Fig. 2b). This allowed to assess changes in the configuration and position of storm  
152 ramparts and sediment transport from the intertidal to the coastal zone between February 2017  
153 and March 2018.

154





Source: ESRI, DigitalGlobe, GeoEye, Earthstar Geographics, CNES/Airbus DS, USDA, USGS, AEX, Getmapping, Aerogrid, IGN, IGP, swisstopo, and the GIS User Community. Images Pleiades of the 11/06/2015, 23/10/2016 and 29/04/2017. © CNES\_2015\_2016\_2017, Airbus DS Distribution, all rights reserved.

155

156 Figure 2. Location of study area and study island sections.

157 a and b show the coverage of the satellite images used in this study. In a, the green, yellow and red boxes

158 indicate 2015, 2016 and 2017 image coverage, respectively. b shows the subdivision of the study area into three

159 distinct areas (i.e. 1, 2 and 3), and the extent of the no data area (corresponding to the airstrip, excluded from the  
160 analysis). It also shows the location of some places of interest cited in the text.

161

## 162 **3.2. Multi-date satellite image analysis**

### 163 **3.2.1. Image acquisition and preparation**

#### 164 **Shoreline change analysis**

165 The satellite images used in this study were obtained from Airbus Defence and Space  
166 archives. Due to image availability constraints, we had to use two different images to  
167 characterise the pre-event situation and to restrict the study area to the northeastern part of the  
168 atoll extending from Garuae Pass to the south of the inhabited area (Fig. 2a). The pre-event  
169 images were acquired on 11 June 2015 (northeastern part of the atoll, including the inhabited  
170 area) and 23 October 2016 (central northern part of the atoll, including Garuae Pass and most  
171 of the airstrip), i.e. respectively eight and four months before the event (Table 1). The post-  
172 cyclone image was taken on 29 April 2017, i.e. approximately two months and a half after the  
173 event. We verified that no wave event had occurred in these two intervals. In addition, we  
174 checked the relative stability of the shoreline during fair weather periods, using the June 2015  
175 and October 2016 images (see SM1). These checks confirmed that available images could be  
176 used to assess the impacts of tropical low 13F. The resolution of the images (0.5 m) and  
177 image quality were satisfactory for shoreline change digitisation. In addition, the UAV  
178 images taken on 10 March 2018 were assembled into an orthomosaic and georeferenced in  
179 ArcGIS 10.5.1 using ground control points extracted from the April 2017 Pléiades satellite  
180 image.

Date	Sensor	Type	Pixel size
11/06/2015	Pléiades-1B	Multispectral	2 m
11/06/2015	Pléiades-1B	Panchromatic	0.5 m
23/10/2016	Pléiades-1A	Multispectral	2 m
23/10/2016	Pléiades-1A	Panchromatic	0.5 m
29/04/2017	Pléiades-1B	Multispectral	2 m
29/04/2017	Pléiades-1B	Panchromatic	0.5 m

10/03/2018	UAV	RGB image	0.045 m
------------	-----	-----------	---------

181 Table 1. Characteristics of the images used in this study.

182 **Sediment deposits and vegetation density analysis**

183 The analysis of sediment deposits and of the coastal vegetation density required the  
184 generation of pan-sharpening images. These images were generated using the Gram Schmidt  
185 Pan-sharpening algorithm (Laben and Brower, 2000) and ENVI 5.4 software. They have a  
186 spatial resolution of 0.5 m, and were obtained by the fusion of the multispectral images at 2 m  
187 resolution with the panchromatic image at 0.5 m. Because the 2015 and 2016 pan-sharpening  
188 images had offsets with the 2017 pan-sharpening image, registration was made in ArcGIS  
189 10.5.1 by translation, using geomorphic features as ground control points (2015 translation:  
190 X= -1.5 m, Y = -5 m; 2016 translation: X= -2.5 m, Y = -0.5 m).

191

192 **3.2.2. Image analysis**

193 **Shoreline change assessment**

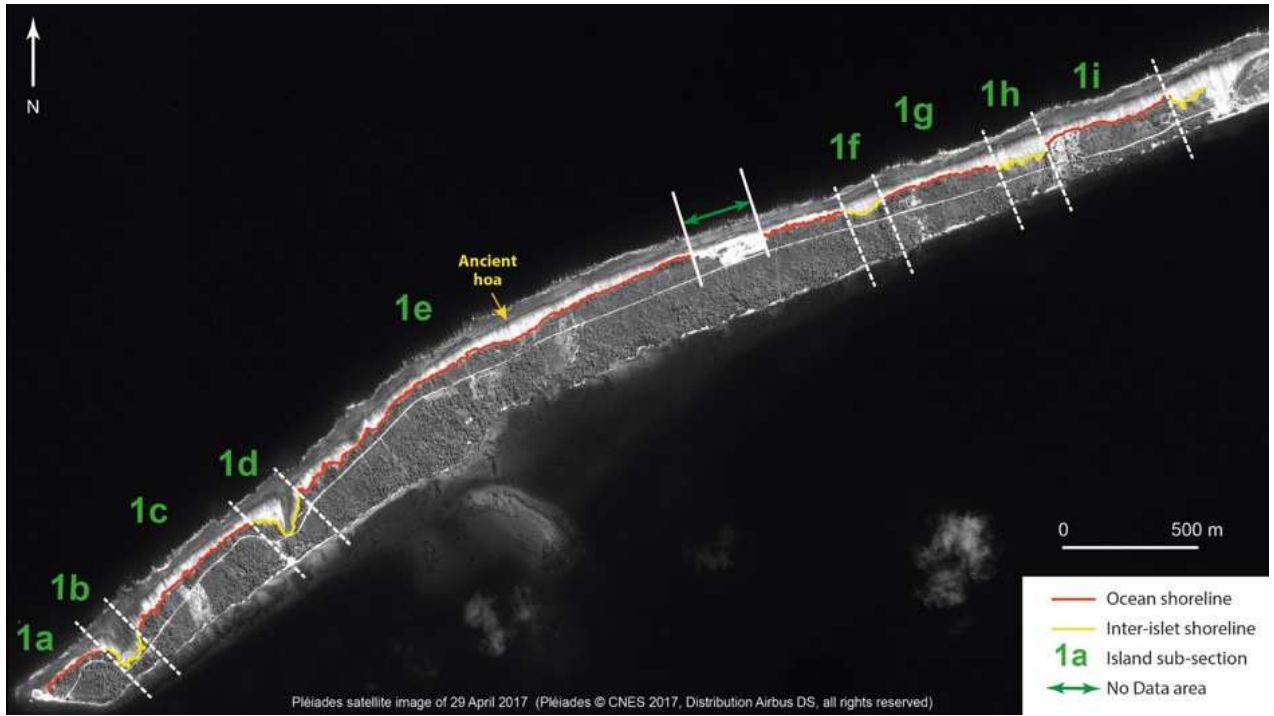
194 We divided the study ocean-facing shoreline into three shoreline sections from west to east,  
195 numbered 1, 2 and 3 (Fig. 2b). Shoreline section 1 was divided into sub-sections to account  
196 for the alternation of ocean-facing shoreline (1a, 1c, 1e, 1g and 1i) and hoa-type shoreline (1b,  
197 1d, 1f and 1h) (Fig. 3). This was not done for shoreline sections 2 and 3 which only include  
198 ocean-facing shoreline. In line with previous studies assessing the impact of storm events on  
199 shoreline position (Ford and Kench, 2014, 2016; Duvat et al., 2017a, 2017b), we used the  
200 vegetation line as a shoreline proxy (Fig. 4). Along some shoreline sections, especially in the  
201 vicinity of hoa, a low-density vegetation cover generally occurs that extends seaward over  
202 great distances. In such configurations, we excluded the area covered with scattered plants  
203 from the island boundary, considering the continuous vegetated part of islands to correspond  
204 to their stable area (Fig. 4c). In addition, digitising the vegetation line was made impossible  
205 (i.e. no data areas) by vegetation removal in some areas, especially along the airstrip (Fig. 2b)

206 and in a quarry area (Fig. 3). To ensure data consistency and quality, the vegetation line was  
207 digitised by a single operator and at a fixed and adequate scale of 1:800 (Holdaway and Ford,  
208 2019). Using a second and complementary shoreline indicator to the vegetation line, i.e. the  
209 base of the beach, was made impossible as the latter was not detectable due to extensive  
210 sediment spreading in the intertidal area.

211 The errors generated by the three sources of uncertainty to be considered when interpreting  
212 shoreline change from satellite imagery – image resolution (pixel size), image georeferencing  
213 and shoreline digitization (Ford, 2012, 2013; Yates et al., 2013) – were estimated to be 0.5 m,  
214 0.35 m (due to the residual error resulting from the initial offset between the April 2017  
215 image and other images), and <2 m for the digitisation of the vegetation line. The total  
216 vegetation line position error was therefore estimated to be  $\leq 2.85$  m. Shoreline change was  
217 calculated using the Digital Shoreline Analysis System (DSAS) (Thieler et al., 2009), based  
218 on the generation of 10 m interval transects from the baseline. The Net Shoreline Movement  
219 (NSM), measuring the distance between two distinct shorelines, was automatically generated  
220 for all time series (2015-2016, 2016-2017 and 2015-2017) and shoreline sections (1a-1i, 2 and  
221 3). Transects showing changes  $\leq -2.85$  m and  $\geq +2.85$  m respectively indicate a retreat and an  
222 advance of the vegetation line.

223

224

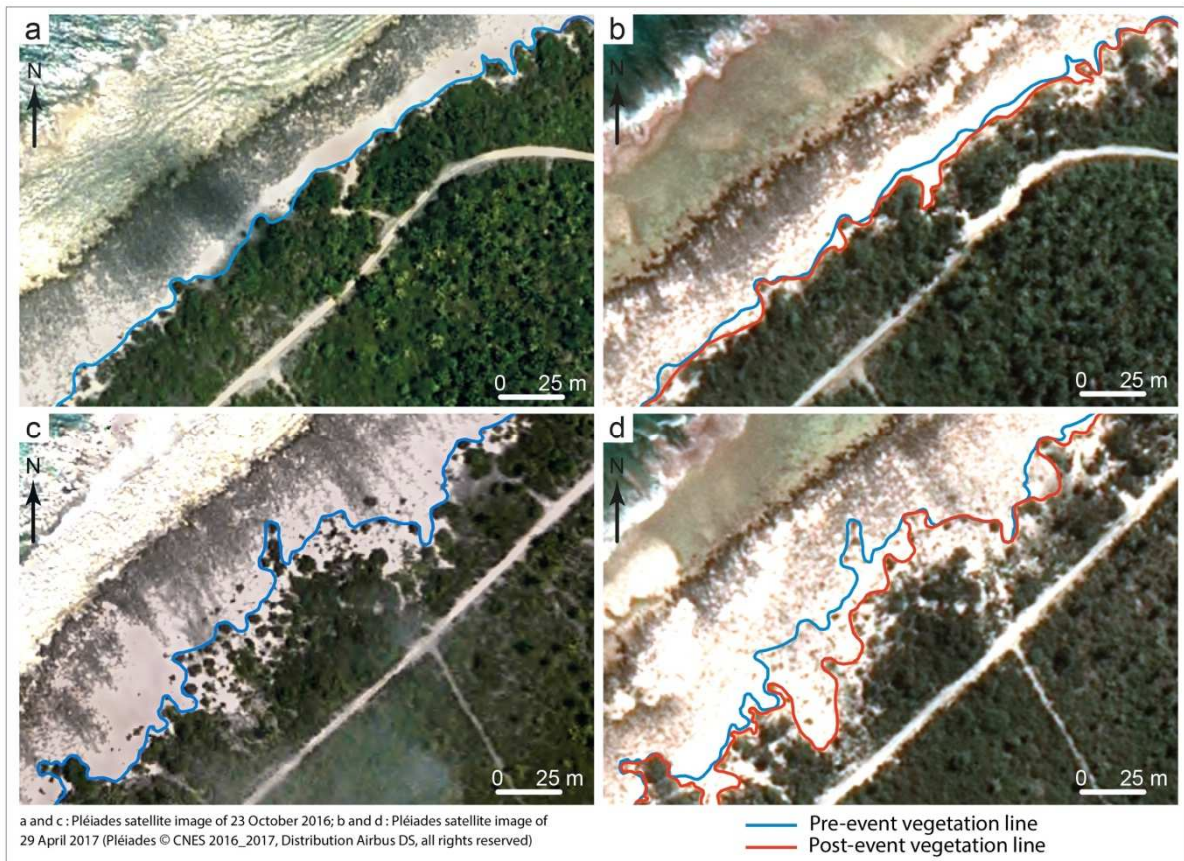


225

226 Figure 3. Subdivision of island section 1.

227 This map shows the subdivisions used to generate shoreline change results, and the differentiation between

228 ocean-facing (in red) and hoa-facing (in yellow) shoreline. The no data area corresponds to a quarry area.



229

230 Figure 4. Shoreline indicator used in this study.

231 We used the vegetation line as a shoreline proxy, and excluded scattered vegetation. a and c illustrate the  
232 digitisation of the pre-storm vegetation line in high- and low-density areas, respectively. b and d show the  
233 position of the pre- and post-storm vegetation line in the same areas as a and c.

234

### 235 **Analysis of storm-generated sediment deposits**

236 The assessment of storm-induced sediment deposits involved (i) field observations, to  
237 describe and geolocate sediment deposits, including those located under the vegetation cover;  
238 (ii) the comparative analysis of the April 2017 (i.e. post-storm) image and the March 2018  
239 (+ ~11 months) UAV orthomosaic, to analyse changes in the configuration (i.e. shape and  
240 area) and position (i.e. migration) of storm ramparts (see SM2 for details); and (iii)  
241 classification methods performed on pan-sharpening images using ENVI software, to map  
242 changes in the extent of sediment deposits over the period covered by the images. The  
243 methodological approach (see SM4) involves Principal Component Analysis (Byrne *and al.*,  
244 1980; Richards, 1999; Chuvieco, 2016) and multistage unsupervised K-means classifications  
245 (Tou and Gonzalez, 1974; Jain, 2010).

246

### 247 **Vegetation analysis**

248 The Normalised Difference Vegetation Index (NDVI) was applied to the pan-sharpening  
249 images to assess coastal vegetation density within a 100 m-wide coastal strip extending  
250 landward from the vegetation line. The values obtained are theoretically comprised between –  
251 1 and +1, with the negative values corresponding to surfaces other than vegetation cover, such  
252 as water or clouds, for which the reflectance in the red is greater than that of the near infrared.  
253 While for bare soils the NDVI has values close to 0 (because the reflectances have the same  
254 order in the red and the near infrared), the vegetation formations have positive values of

255 NDVI, generally comprised between 0.1 and 0.7, and increasing with vegetation density  
256 (Tucker, 1979).

257

## 258 **4. Results**

### 259 **4.1. Storm wave-induced shoreline change**

260 The impact of storm waves on shoreline position decreased eastward, from the highly-  
261 exposed islands located immediately to the east of Garuae Pass to the sheltered village area.  
262 Shoreline section 1, which was the most exposed to wave action due to its location and to its  
263 SW-NE orientation, predominantly exhibited shoreline retreat, which was detected along  
264 54.14% of transects, and secondarily exhibited shoreline stability, noted along 45.86% of  
265 transects. Shoreline retreat was marked in its central part (corresponding to sub-sections 1e, 1f  
266 and 1g), where 51.11 to 93.33% of transects exhibited retreat (Table 2 and SM3) and where  
267 the lowest average and minimum NSM values were respectively comprised between –  
268 12.78 m (1f) and –45.46 m (1e). In contrast, the western part (sub-sections 1a, 1b, 1c and 1d)  
269 and eastern end (1h) of shoreline section 1 predominantly showed shoreline stability, which  
270 was detected along 55.00 (1d) to 85.19% (1a) of transects. In general, the shoreline sections  
271 did not exhibit higher retreat values compared to ocean-facing shoreline sections. Shoreline  
272 sections 2 and 3 predominantly experienced stability, which was detected along 62.72% and  
273 97.65% of transects, respectively. Along shoreline section 2, 36.56% of transects showed  
274 retreat.

275 Beyond general trends, i.e. the prevalence of retreat and stability, respectively, along  
276 shoreline sections 1 and 2, these two shoreline sections showed high alongshore variability in  
277 shoreline response, with some transects exhibiting a marked retreat while others (sometimes  
278 nearby transects) exhibited stability (Table 2). The lowest NSM values obtained were <–17 m  
279 for 6 out of the 9 sub-sections of shoreline section 1 and of –26.13 m for shoreline section 2.

280 The almost absence of erosional transects along shoreline section 3 reflects its sheltered  
 281 position in relation to the storm waves. These results reflect the significant impact of these  
 282 storm waves on the exposed, i.e. north-facing, ocean coast of the atoll.

283

Sub-sections	Number of transects	Mean NSM (m)	Min. NSM (m)	Max. NSM (m)	Accretional transects		Stable transects		Erosional transects	
					Nb	%	Nb	%	Nb	%
1a	27	-1.31	-7.09	0.00	0	0.00	23	85.19	4	14.81
1b*	13	-2.19	-9.19	0.17	0	0.00	10	76.92	3	23.08
1c	59	-3.35	-19.76	0.09	0	0.00	37	62.71	22	37.29
1d*	20	-4.79	-30.77	0.00	0	0.00	11	55.00	9	45.00
1e	210	-6.36	-45.46	2.75	0	0.00	70	33.33	140	66.67
1f*	15	-12.78	-33.91	-2.43	0	0.00	1	6.67	14	93.33
1g	45	-3.70	-14.08	0.00	0	0.00	22	48.89	23	51.11
1h*	32	-4.74	-31.21	0.00	0	0.00	21	65.63	11	34.37
1i	50	-5.37	-17.03	0.03	0	0.00	21	42.00	29	58.00
Total 1a-1i	471	/	/	/	0	0.00	216	45.86	255	54.14
2	279	-3.01	-26.13	4.13	2	0.72	175	62.72	102	36.56
3	339	0.56	-3.64	3.93	7	2.06	331	97.65	1	0.29

284 Table 2 – Changes in the position of the vegetation line on ocean and inter-islet channel shores over  
 285 the 2015-2017 period. \*sub-sections correspond to inter-islet shoreline.

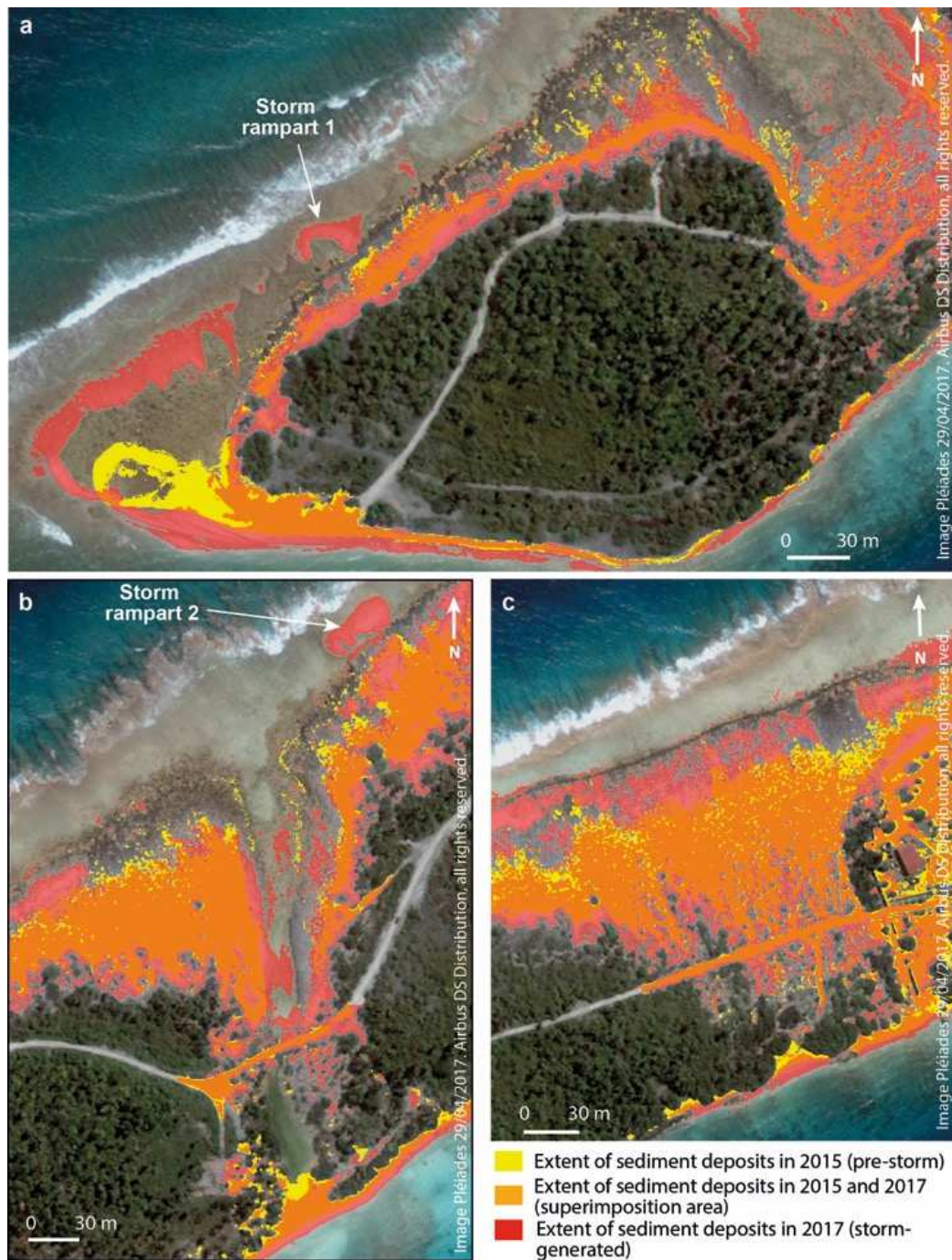
286

#### 287 4.2. The predominance of constructional vs. erosional impacts

288 Tropical low 13F caused extensive sediment injection into the intertidal area, that is, on the  
 289 conglomerate platform (Figs. 5 and 6), as a result of the (i) mechanical destruction on the  
 290 outer slopes (confirmed by the diving instructors interviewed) and transfer to the  
 291 conglomerate platform of living corals (Fig. 6c), (ii) transfer of loose material, especially sand  
 292 and smooth and rounded coral rubble and blocks from the spur and groove reservoir to the  
 293 conglomerate platform (Figs. 6a, 6b, 8), and (iii) dismantling of the conglomerate platform,



294 which provided sand and smooth and rounded coral rubble and blocks that were transferred to  
295 the coast (Fig. 6d). Extensive sand and rubble sheets and tracts formed (Figs. 5 and 6a, 6b),  
296 stretching from the seaward boundary of the conglomerate platform where no sediment  
297 accumulation was present before the event to the coast and even to interior areas, especially  
298 where shore-perpendicular tracks facilitated wave penetration (Fig. 5a). Although this was not  
299 measurable, in March 2018, we noted significant landward transfer of the sediment that had  
300 initially accumulated on the seaward edge of the conglomerate platform. Additionally, this  
301 storm event reactivated some non-functional hoas (Figs. 5b, 5c). Moreover, massive sand and  
302 rubble accumulation occurred on the east-west track connecting islands between Garuae Pass  
303 and Rotoava, which reached up to 100 m landward from the vegetation line.



304

305 Figure 5. Mapping of pre-storm and post-storm sediment deposits, including superimposition

306 areas.

307 These maps highlight (in red) the extent of storm-generated sediment deposits in intertidal (including sediment

308 sheets and tracts and the formation of two storm ramparts), coastal and inland areas. a shows massive sediment

309 injection from the spur and groove system onto the narrow (~50 m here) conglomerate platform nearby Garuae

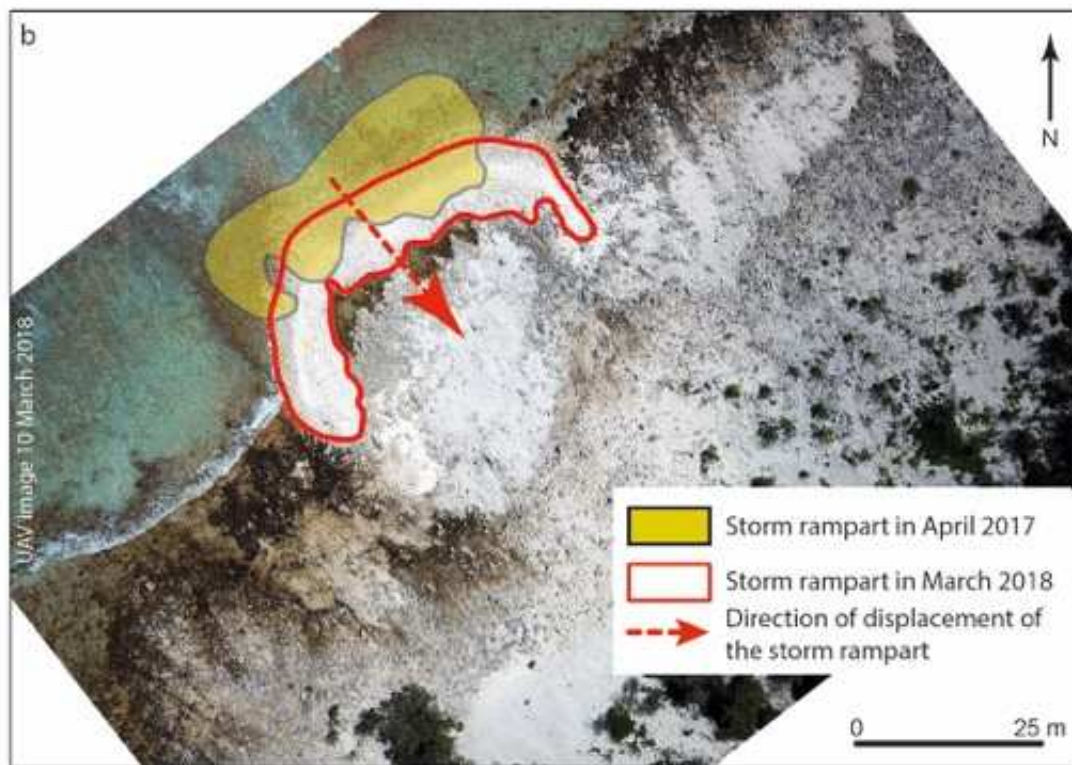
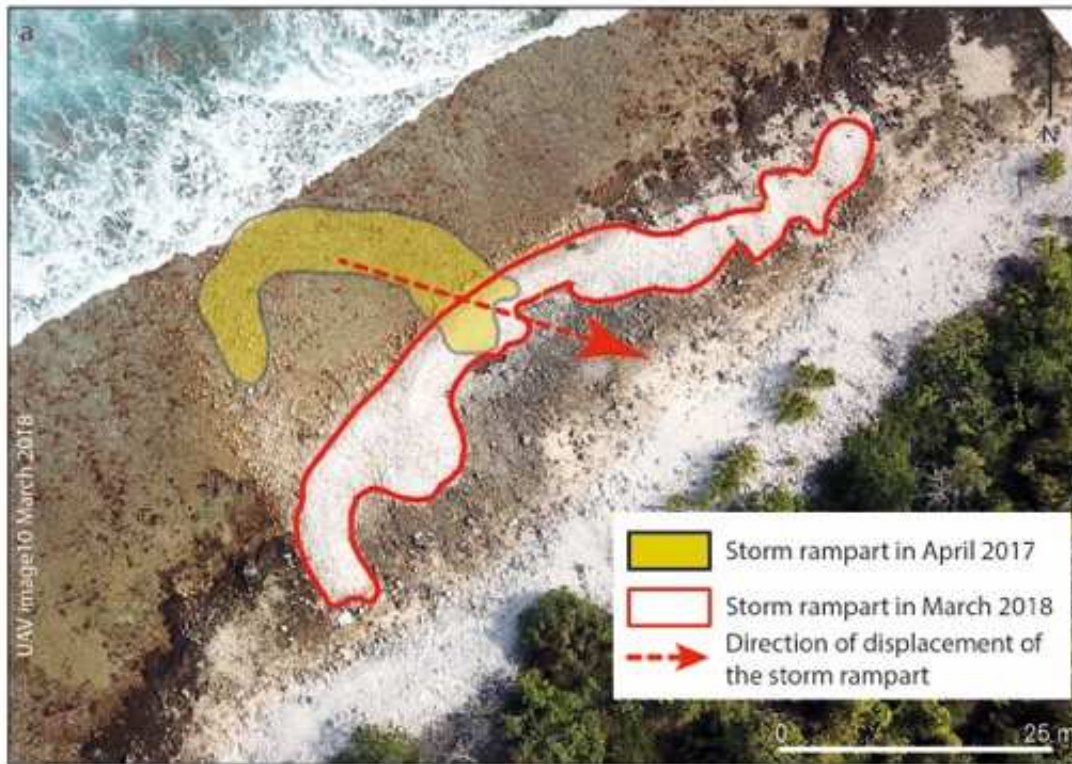
310 Pass. b and c illustrate the injection of sediments on the outer, i.e. seaward, border of the conglomerate platform

311 that showed no sediment accumulation before the event; they also emphasise ocean-to-island sediment transfer  
312 through hoa (b) and in ancient hoa (c)



313  
314 Figure 6. Accretional impacts of tropical low 13F.  
315 a and b show sediment sheets. c illustrate living coral inputs from the spur and groove reservoir. d show  
316 important sediment inputs in a non-vegetated area and induced sediment accumulation on the main track that  
317 connects western islands to the village.  
318

319 Importantly, this event led to the formation of two small storm ramparts on the seaward edge  
320 of the conglomerate platform (Figs. 7 and 8) in shoreline section 1 (i.e. the most exposed to  
321 the storm waves). These ramparts respectively formed at a distance of ~83 m (R1) and  
322 ~1.3 km (R2) from Garuae Pass (see location in Fig. 2). At the time of their formation, R1 and  
323 R2 respectively measured 30 and 41 m in their longest axis, had maximum heights of ~1.30 m  
324 and ~2.0 m, and a surface area of ~229.52 m<sup>2</sup> and ~593.08 m<sup>2</sup>. They were principally  
325 composed of small coral debris (5-10 cm in diameter), mixed up with coral blocks measuring  
326 30 to 50 cm in diameter. The material composing these two ramparts was a mix of fresh  
327 corals and loose (and smooth) rubble. After one year, these two ramparts had undergone  
328 major changes in configuration and position. Both showed important sediment reworking and  
329 landward migration. In March 2018, R1 had considerably lengthened (from 30 to 80 m in its  
330 longest axis, area of 412.96 m<sup>2</sup>), while its centre of gravity had moved landward by 23.1 m. In  
331 the same time, R2 underwent more limited changes in shape and position, as its length  
332 increased from 41 to 48 m (area of 599.95 m<sup>2</sup>) while its landward migration was limited to  
333 10.7 m.



334

335 Figure 7. Changes in the configuration and position of the storm ramparts after one year.

336 a shows R1, which formed at a distance of ~83 m from Garuae Pass and underwent marked changes in shape and

337 position. b shows R2, which was more massive and underwent limited changes in configuration and position,

338 despite, like R1, a significant landward migration.



339

340 Figure 8. Storm ramparts one year after their formation (March 2018).

341 a shows the longitudinal profile of R1, while b and c illustrate the more massive character of R2. d shows the

342 material composing R2.

343

344 Tropical low 13F also caused marked erosion, including in the intertidal area, where the  
345 waves caused the dismantling and scouring of the conglomerate platform, both in its outer  
346 (Fig. 9a) and inner (Fig. 9b) parts, and in the coastal area, where wave attack caused not only  
347 the retreat of the vegetation line, but also localised soil scouring. However, on the whole, the  
348 areas experiencing sediment deposition predominated.



349

350 Figure 9. Erosional impacts of tropical low 13F on the conglomerate platform.

351 a illustrates the contribution of storm waves to the dismantling of the outer part of the conglomerate platform  
352 and transfer of the smooth coral rubble and blocks removed from this platform to the shore. b shows that the  
353 dismantling and scouring of this platform also occurred in its inner part, where it connects to the base of the  
354 beach.

355

### 356 **4.3. Interferences of human activities with storm-driven processes**

357 In the study area, the major mode of interference of human activities with storm-driven  
358 processes relates to the degradation, i.e. either partial or total destruction, depending on  
359 locations, of the coastal vegetation belt composed of native species, which exacerbated wave  
360 incursion inland. This was observed first, in the airstrip area (see location in Fig. 2a), where  
361 the removal of the vegetation on both sides of the airstrip for security purposes allowed the  
362 waves to cross over the island from ocean to lagoon, which caused extensive sediment  
363 deposition on the airstrip (Fig. 10a). The same phenomenon, i.e. extensive overwash causing  
364 massive sediment deposition, occurred in the quarry area (see location in Fig. 2a), where the  
365 nearly total destruction of the coastal vegetation over a 70 m-wide and 300 m-long area  
366 generated massive sediment accumulation, including on the west-east track and in the  
367 vegetated area extending landward from this track (Fig. 10b). The waves also penetrated far  
368 inland in the axis of the shore-perpendicular tracks connecting the ocean-side beaches to the  
369 west-east track (Fig. 10c). In most depositional areas, sediment deposits, which consisted of  
370 sand, coral debris and blocks, were a few centimetres thick. However, we also observed  
371 sediment deposits reaching up to a few decimetres in thickness, especially in the extension of  
372 ho, on the west-east track and on some shore-perpendicular tracks.

373





374

375 Figure 10. Interferences of human activities with storm-driven processes.

376 a illustrates the impacts of the storm waves on the airstrip, i.e. extensive sediment deposition resulting from the

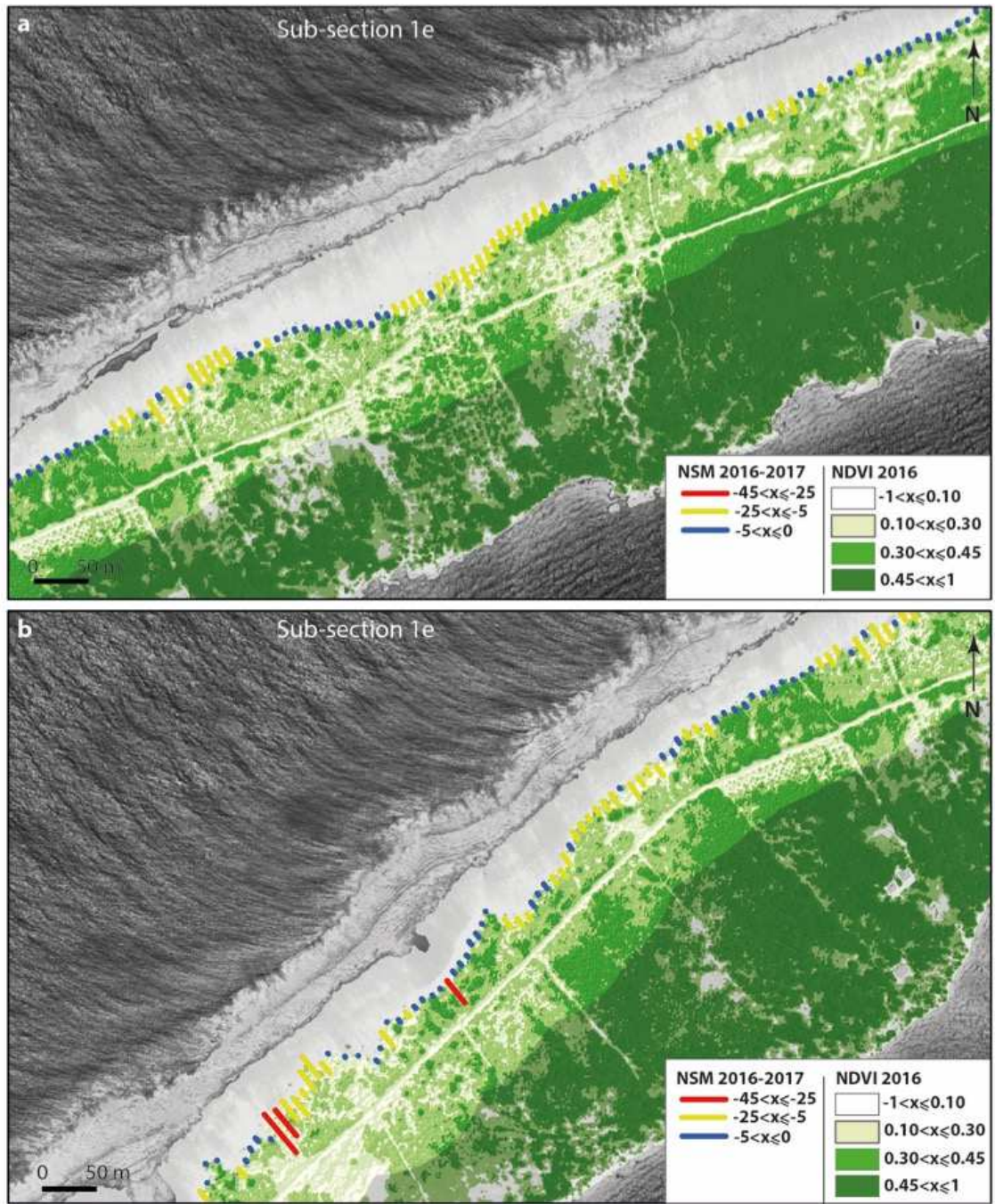
377 removal of the coastal vegetation. b shows the exacerbation of overwash processes and associated sediment

378 deposition in the quarry area, where the coastal vegetation has been extensively removed. c illustrates extensive

379 wave incursion inland in the axis of shore-perpendicular tracks.

380

381 Furthermore, Net Shoreline Movement (NSM, i.e. distance between the pre- and post-storm  
382 vegetation line position) values are generally (although not systematically) in accordance with  
383 NDVI values indicating pre-storm vegetation density (Figs. 11). The highest NSM values (i.e.  
384 comprised between 0 and -5 m and indicating limited shoreline retreat) correspond to the  
385 highest (i.e. reaching up to 0.56) NDVI values indicating high vegetation density (Fig. 12).  
386 Conversely, the lowest NSM values (comprised between -25 and -45 m and indicating  
387 marked shoreline retreat) correspond to the lowest (i.e. <0.35) NDVI values indicating low  
388 vegetation density. These findings indicate that a dense coastal vegetation belt composed of  
389 native species is more resistant to storm waves than a low-density vegetation cover. We also  
390 observed that where the coastal vegetation belt was dense, soil scouring was limited and  
391 sediment deposition was important and restricted to a 10-to-20 m wide coastal strip. This  
392 confirms the major role of a healthy coastal vegetation belt in protecting soils from storm-  
393 induced scouring and in promoting beach ridge building.  
394

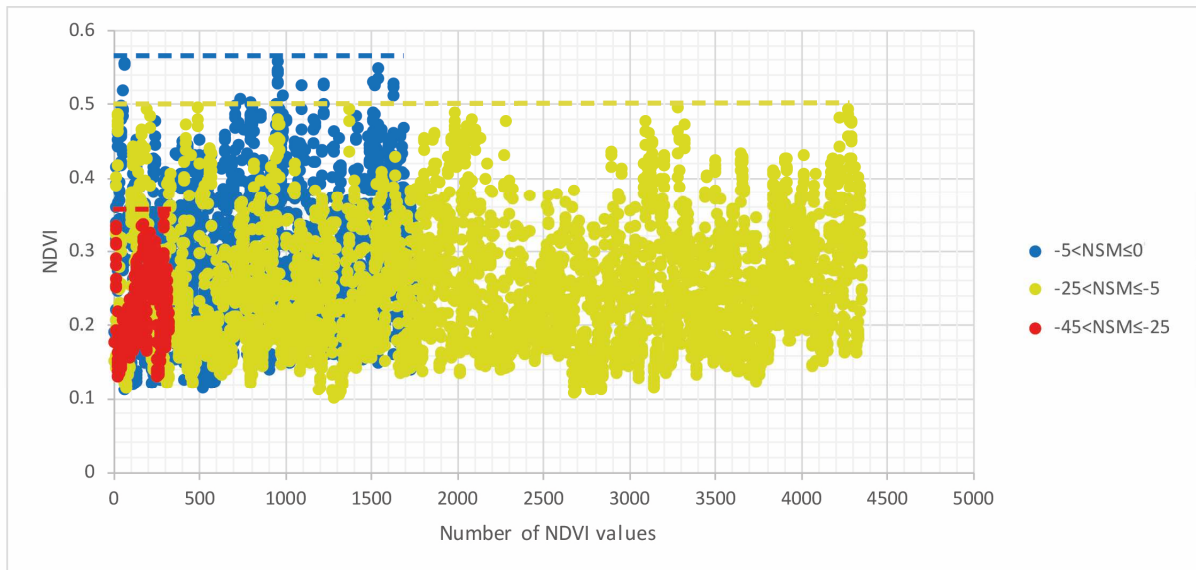


395

396 Figure 11. Relationship between shoreline response and coastal vegetation density.

397 a and b show that Net Shoreline Movement (NSM) values, which reflect shoreline response, are the smaller

398 where coastal vegetation density (reflected by 0.10 to 1 NDVI values) are the highest and vice versa.



399  
400 Figure 12. Distribution of NDVI values according to NSM values.

401 The highest NSM values (i.e. comprised between 0 and -5 m and indicating limited shoreline retreat)  
402 correspond to the highest (i.e. reaching up to 0.56) NDVI values indicating high vegetation density  
403 (Fig. 12). Conversely, the lowest NSM values (comprised between -25 and -45 m and indicating  
404 marked shoreline retreat) correspond to the lowest (i.e. <0.35) NDVI values indicating low vegetation  
405 density.

406

407

408 **5. Discussion**

409 **5.1. Implications for future research**

410 Moderate climate events such as tropical low 13F have so far been overlooked by geomorphic  
411 studies on atolls, which have focused on the impacts of more spectacular, i.e. high-energy,  
412 climate events, such as tropical cyclones and strong distant-source swells. This study is the  
413 first one that investigates the geomorphic impacts of a moderate climate event. Importantly,  
414 our findings show that such climate events, which are much more frequent than tropical  
415 cyclones – to be precise have a return period of ~ 2-3 years against 39 years for tropical  
416 cyclones in the northwestern Tuamotu atolls – have unexpected and significant geomorphic  
417 impacts on atoll islands. The waves generated by tropical low 13F had marked impacts all  
418 along the north-facing exposed ocean coast of the atoll. However, in the study area, the  
419 vegetation line predominantly exhibited stability, which was detected along 52.13% of  
420 transects, while retreat was observed along 47.60% of transects. This finding, together with  
421 the large extent of constructional features, including sand and rubble sheets and tracts and two  
422 small storm ramparts that all showed significant landward migration after one year, highlights  
423 that such moderate storms mainly have constructional effects. In this case, the storm waves  
424 injected massive sediment inputs into the island system through the mechanical destruction of  
425 living corals on the outer slopes and the transfer of loose and smooth coral rubble and blocks  
426 from the spur and groove reservoir (where these materials had accumulated) and  
427 conglomerate platform, which suffered marked dismantling, to the beaches and even to inland  
428 areas. At several locations, the storm waves even crossed over the islands, reaching the  
429 lagoon. Such extensive impacts, both erosional and accretional, were so far known to be  
430 generated by high-energy climate events such as tropical cyclones and distant-source swells.  
431 This study therefore brings new insights on atoll island change by demonstrating the

432 significant contribution, and especially the accretional impact, of a moderate climate event to  
433 island and shoreline change.

434 Based on these observations, we advocate that extensively assessing the geomorphic impacts  
435 of such events on atoll islands is urgently needed to improve the understanding of atoll island  
436 dynamics. Such knowledge is crucial in the current climate change context, in which climate-  
437 related pressures are rapidly increasing in atoll regions and are expected to cause increased  
438 shoreline retreat and island destabilisation (Beetham et al., 2017; Shope and Storlazzi, 2019;  
439 Tuck et al., 2019). In fact, determining whether relatively frequent moderate climate events –  
440 i.e. not only tropical lows forming in the intertropical zone, but also moderate distant-source  
441 swells that affect the northwestern Tuamotu atolls 2 to 3 times a year according to their  
442 inhabitants – offset the sediment losses caused by extreme climate events seems crucial to  
443 properly understand atoll island change. In those atoll regions where tropical cyclones are  
444 uncommon (e.g. in the Tuamotu Archipelago, Larrue and Chirron, 2010; in the Marshall  
445 Islands, Ford and Kench, 2014, 2016; in the Maldives, Aslam and Kench, 2017), moderate  
446 climate events probably play a more determinant role in island dynamics and change than  
447 extreme climate events. Consequently, increased research efforts are needed on both their  
448 frequency (not only current, but also projected) and their effects on atoll islands.

449

## 450 **5.2. Implications for risk reduction on atolls**

451 Our findings also provide major insights for coastal risk reduction on atolls. Given that the  
452 impacts of moderate climate events, including overwash and extensive sediment deposition,  
453 are significant and may reach the interior of islands, especially in low-lying and non-  
454 vegetated areas, it seems crucial to preserve the coastal vegetation belt which buffers storm  
455 waves and protects inner areas from their devastating effects from human-induced  
456 destruction. The spatial correlations between (i) vegetation density (i.e. condition) and

457 shoreline response – with shoreline retreat being inversely proportional to vegetation density  
458 –, and (ii) vegetation density and the extent of overwash-induced sediment deposition,  
459 advocates for the preservation, and even for the restoration where it has been destroyed, of the  
460 coastal vegetation belt. Removing the coastal vegetation exacerbates shoreline retreat, soil  
461 scouring, while also increasing the extent of overwash and of inland sediment deposition.  
462 Such an exacerbation of storm impacts on both shoreline and island, which was not really  
463 problematic (except on the airstrip) in the present case, would have much more serious  
464 consequences in a densely-settled area. Where atoll reef-island systems keep exhibiting  
465 natural accretional processes, as the ones described in this study, nature-based solutions,  
466 which describe ‘actions to protect, sustainably manage, and restore natural or modified  
467 ecosystems that address societal challenges (e.g. climate change, food and water security or  
468 natural disasters) effectively and adaptively, while simultaneously providing human well-  
469 being and biodiversity benefits’ (Cohen-Shacham et al., 2016: 2), should be prioritised. The  
470 same conclusion arose from previous studies addressing tropical cyclone impacts, which also  
471 highlighted not only the constructional impacts of such events, but also the exacerbation of  
472 coastal erosion and flooding where human activities had led to the entire or partial destruction  
473 of the coastal vegetation belt (Stoddart, 1963, 1965; Duvat et al., 2017a).

474

## 475 **6. Conclusions**

476 The study of the impacts of a moderate climate event, i.e. tropical low 13F, on Fakarava  
477 Atoll, in the northwestern Tuamotu Archipelago, French Polynesia, based on field  
478 observations and multi-date image analysis, brings important new insights to the  
479 understanding of atoll island dynamics. Importantly, it shows that such events, which are  
480 much more frequent than tropical cyclones (return period of 2-3 years against 39 years in the  
481 present case), and have so far been overlooked, (1) have significant geomorphic impacts on

482 atoll islands, and even comparable impacts (at least in nature, e.g. causing shoreline retreat  
483 and the formation of storm ramparts and extensive sediment sheets and tracts on the reef flat)  
484 to those of intense tropical cyclones, (2) contribute to island building through the injection of  
485 massive sediment inputs into the island system, due both to the mechanical destruction of  
486 living corals on the outer slopes and the transfer to the intertidal, coastal and inland areas, of  
487 loose sediments that had accumulated in the spur and groove area and on the conglomerate  
488 platform, (3) have less extensive (i.e. restricted to the intertidal and coastal zones) impacts  
489 where the coastal vegetation belt composed of native species has been preserved, while  
490 reaching inland areas over great distances (>100 m here) where the latter has been destroyed.  
491 This last finding advocates for the promotion of nature-based solutions to face coastal erosion  
492 and flooding in such settings, that is, for the preservation or restoration of the coastal  
493 vegetation, and beyond, for the recognition that a continuum of healthy ecosystems (i.e. from  
494 the reef ecosystem to inland areas, including the coastal vegetation) is required to maintain  
495 coastal risks as low as possible on atoll islands.

496 In addition, these findings call for the more systematic assessment of the impacts of moderate  
497 climate events, as these events, which include not only tropical lows that form in the  
498 intertropical zone but also moderate distant-source swells, are much more frequent than  
499 tropical cyclones, especially (but not only) in atolls areas that are located outside the cyclone  
500 belt such as the Central Pacific (Tuamotu region), the Western (Marshall Islands) and  
501 equatorial Pacific, and the central Indian Ocean (Maldives Islands). For example, in the  
502 Western Tuamotu that are the subject of this study, tropical cyclones have a return period of  
503 ~39 years, while tropical lows and moderate distant-source swells respectively occur every 2-  
504 3 years and 2-3 times a year. This study thus reveals an important research gap in atoll  
505 geomorphic studies, which requires increased scientific efforts in the future, as such  
506 constructional events may, at least in some atoll contexts (i.e. where tropical cyclones are



507 uncommon) offset the potentially erosive (at least at some locations) impacts of increasingly  
508 frequent extreme climate events.

509

## 510 **Acknowledgements**

511

512 This work was supported by the French National Research Agency under the STORISK  
513 research project (No. ANR-15-CE03-0003). The authors warmly thank the municipality and  
514 the inhabitants of Fakarava for providing highly valuable information during the conduction  
515 of this study.

516

## 517 **References**

518 Andrefouët, A., Ardhuin, F., Queffeulou, P., Legendre, R., 2012. Island shadow effects and the wave  
519 climate of the Western Tuamotu Archipelago (French Polynesia) inferred from altimetry and  
520 numerical model data. *Mar. Pollut. Bull.* 65: 415-424.

521 <http://dx.doi.org/10.1016/j.marpolbul.2012.05.042>.

522 Aslam, M., Kench, P.S., 2017. Reef island dynamics and mechanisms of change in Huvadho Atoll,  
523 Republic of the Maldives, Indian Ocean. *Anthropocene* 18: 57-68.

524 <http://dx.doi.org/10.1016/j.ancene.2017.05.003>.

525 Baines, G. B.K., Beveridge, P.J., Maragos, J.E., 1974. Storms and island building at Funafuti Atoll,  
526 Ellice Islands, *Proc. 2<sup>nd</sup> Intern. Coral Reef Symp.*, Vol. 2: 485-496.

527 Baines, G. B.K., McLean, R. F., 1976. Sequential studies of hurricane deposit evolution at Funafuti  
528 Atoll. *Mar. Geol.* 21: 1–8. [http://dx.doi.org/10.1016/0025-3227\(76\)90097-9](http://dx.doi.org/10.1016/0025-3227(76)90097-9).

529 Becker, M., Meyssignac, B., Letetrel, C., Llovel, W., Cazenave, A., Delcroix, T., 2012. Sea level  
530 variations at tropical Pacific islands since 1950. *Glob. Planet. Chang.* 80–81: 85–98.

531 <http://dx.doi.org/10.1016/j.gloplacha.2011.09.004>.

532 Beetham, E., Kench, P. S., Popinet, S., 2017. Future Reef Growth Can Mitigate Physical Impacts of  
533 Sea-Level Rise on Atoll Islands, *Earth's Future* 5, 1002–1014.  
534 <http://dx.doi.org/10.1002/2017EF000589>.

535 Byrne, G. F., Crapper, P. F., Mayo, K. K. 1980. Monitoring land-cover change by Principal  
536 Component Analysis of multitemporal data. *Remote Sens. Environ.* 10, 175–184.  
537 [https://doi.org/10.1016/0034-4257\(80\)90021-8](https://doi.org/10.1016/0034-4257(80)90021-8)

538 Canavesio, R., 2019. Distant swells and their impacts on atolls and tropical coastlines. The example of  
539 submersions produced by lagoon water filling and flushing currents in French Polynesia during  
540 1996 and 2011 mega swells. *Glob. Planet. Chang.* 177, 116-126.  
541 <http://dx.doi.org/10.1016/gloplacha.2019.03.018>.

542 Church, J.A., White, N.J., 2011. Sea-level rise from the late 19th to the early 21st century. *Surv.*  
543 *Geophys.* 32:585–602. <http://dx.doi.org/10.1007/s10712-011-9119-1>.

544 Chuvieco, E., 2016. *Fundamentals of Satellite Remote Sensing: An Environmental Approach*. 2nd ed.  
545 CRC Press. ISBN : 9781498728058

546 Cohen-Shacham, E., Walters, G., Janzen, C., Maginnis, S. (eds.), 2016. *Nature-based Solutions to*  
547 *address global societal challenges*. Gland, Switzerland: IUCN. xiii + 97pp.

548 Duvat, V., Pillet, V., 2017. Shoreline changes in reef islands of the Central Pacific: Takapoto Atoll,  
549 Northern Tuamotu, French Polynesia. *Geomorphology* 282:96–118.  
550 <https://dx.doi.org/10.1016/j.geomorph.2017.01.002>.

551 Duvat, V.K.E., Volto, N., Salmon, C., 2017a. Impacts of category 5 tropical cyclone Fantala (April  
552 2016) on Farquhar Atoll, Seychelles Islands, Indian Ocean. *Geomorphology* 298: 41-62.  
553 <http://dx.doi.org/10.1016/j.geomorph.2017.09.022>.

554 Duvat, V.K.E., Salvat, B., Salmon, C., 2017b. Drivers of shoreline change in atoll reef islands of the  
555 Tuamotu Archipelago, French Polynesia. *Glob. Planet. Chang.* 158: 134-154.  
556 <http://dx.doi.org/10.1016/j.gloplacha.2017.09.016>.

557 Duvat, V.K.E., Magnan, A.K.M., Canavesio, R., 2018. La reconstruction de chaînes d'impacts au  
558 service de l'évaluation de la résilience des territoires et de la réduction des risques météo-marins :

559 le cas des atolls des Tuamotu, Polynésie française. *La Houille Blanche* 2, 13-21.  
560 <https://doi.org/10.1051/lhb/2018016>

561 Ford, M., 2012. Shoreline changes on an urban atoll in the central Pacific Ocean: Majuro Atoll,  
562 Marshall Islands. *J. Coast. Res.* 28:11–22. <https://doi.org/10.2112/JCOASTRES-11-00008.1>.

563 Ford, M., 2013. Shoreline changes interpreted from multi-temporal aerial photographs and high  
564 resolution satellite images: Wotje Atoll, Marshall Islands. *Remote Sens. Environ.* 135:130–140.  
565 <https://doi.org/10.1016/j.rse.2013.03.027>.

566 Ford, M.R., Kench, P.S., 2014. Formation and adjustment of typhoon-impacted reef islands interpreted  
567 from remote imagery: Nadikdik Atoll, Marshall Islands. *Geomorphology* 214, 216–222.  
568 <http://dx.doi.org/10.1016/j.geomorph.2014.02.006>.

569 Ford, M.R., Kench, P.S., 2016. Spatiotemporal variability of typhoon impacts and relaxation on Jaluit  
570 Atoll, Marshall Islands. *Geology* 44(2), 159-162. <http://dx.doi.org/10.1130/G37402.1>.

571 Hoeke, R.K., McInnes, K.L., Kruger, J., McNaught, R., Hunter, J., Smithers, S., 2013. Widespread  
572 inundation of Pacific islands by distant-source wind-waves. *Glob. Environ. Chang.* 108: 128-138.  
573 <http://dx.doi.org/10.1016/j.gloplacha.2013.06.006>.

574 Holdaway, A., Ford, M., 2019. Resolution and scale controls on the accuracy of atoll island shorelines  
575 interpreted from satellite imagery. *Applied Geomatics*. [http://dx.doi.org/10.1007/s12518-019-](http://dx.doi.org/10.1007/s12518-019-00266-7)  
576 [00266-7](http://dx.doi.org/10.1007/s12518-019-00266-7).

577 ISPF (Institut Statistique de la Polynésie française) 2017. Statistical data of French Polynesia.  
578 <http://www.ispf.pf/>

579 Jain, A.K., 2010. Data clustering: 50 years beyond K-means. *Pattern Recognition Letters* 31(8), 651-  
580 666. <https://doi.org/10.1016/j.patrec.2009.09.011>

581 Kench, P.S., McLean, R., Brander, R., Nicholl, S.L., Smithers, S., Ford, M., Parnell, K.E., Aslam, M.,  
582 2006. Geological effects of tsunami on mid-ocean atoll islands: the Maldives before and after the  
583 Sumatran tsunami. *Geology* 34(3). <http://dx.doi.org/10.1130/G21907.1>.

584 Laben C.A., Brower B.V., 2000. Process for enhancing the spatial resolution of multispectral imagery  
585 using pan-sharpening. Google Patents.

586 Larrue, S., Chiron, T., 2010. Les îles de Polynésie française face à l'aléa cyclonique. *Vertigo* 10 (3).  
587 <http://vertigo.revues.org/10558>.

588 Laurent, V., Varney, P., 2014. Historique des cyclones de Polynésie Française de 1981 à 2010. *Météo-*  
589 *France Direction interrégionale de la Polynésie Française, Etudes et Climatologie, Tahiti, 175 p.*

590 Le Cozannet, G., Garcin, M., Petitjean, L., Cazenave, A., Becker, M., Meyssignac, B., Walker, P.,  
591 Devilliers, C., Le Brun, O., Lecacheux, S., Baills, A., Bulteau, T., Yates, M., Wöppelmann, G.,  
592 2013. Exploring the relation between sea level rise and shoreline erosion using sea level  
593 reconstructions: an example in French Polynesia. *J. Coast. Res.* 65, 2137-2142.  
594 <https://doi.org/10.2112/SI65-361.1>

595 Maragos J. E., Baines G. B. K., Beveridge P. J., 1973. Tropical Cyclone Bebe Creates a New Land  
596 Formation on Funafuti Atoll. *Science* 181 (4105), 1161-1164.  
597 <http://dx.doi.org/10.1126/science.181.4105.1161>.

598 Nurse, L.A., McLean, R.F., Agard, J., Briguglio, L.P., Duvat-Magnan, V., Pelesikoti, N., Tompkins,  
599 E., Webb, A., 2014. Small islands. In: Barros, V.R., Field, C.B., Dokken, D.J., Mastrandrea, M.D.,  
600 Mach, K.J., Bili, T.E., Chatterjee M., Ebi, K.L., Estrada, Y.O., Genova, R.C., Girma, B., Kissel,  
601 E.S., Levy, A.N., MacCracken, S., Mastrandrea, P.R., White, L.L. (Eds.), *Climate Change 2014:*  
602 *Impacts, Adaptation and Vulnerability. Part B: Regional Aspects. Contribution of Working Group*  
603 *II to the Fifth Assessment Report of the Intergovernmental Panel on Climate Change. Cambridge*  
604 *University Press, Cambridge and New York, pp.1613–1654.*

605 Pirazzoli, P.A., Montaggioni, L.F., 1986. Late Holocene sea-level changes in the northwest Tuamotu  
606 islands, French Polynesia. *Quaternary Research* 25(3), 350-368. [http://dx.doi.org/10.1016/0033-](http://dx.doi.org/10.1016/0033-5894(86)90006-2)  
607 [5894\(86\)90006-2](http://dx.doi.org/10.1016/0033-5894(86)90006-2).

608 Rankey, E. C., 2011: Nature and stability of atoll island shorelines: Gilbert Island chain, Kiribati,  
609 equatorial Pacific. *Sedimentology* 58 (7), 1831-1859. [http://dx.doi.org/10.1111/j.1365-](http://dx.doi.org/10.1111/j.1365-3091.2011.01241.x)  
610 [3091.2011.01241.x](http://dx.doi.org/10.1111/j.1365-3091.2011.01241.x).

611 Richards, J.A., Jia, X. 2006. *Remote Sensing Digital Image Analysis: An Introduction*, Springer-  
612 *Verlag, Berlin Heidelberg, 439 p.*

613 Rougerie, F., 1994. Nature et fonctionnement des atolls des Tuamotu (Polynésie Française).  
614 *Oceanologica Acta* 18(1), 61–78.

615 Scoffin, T.P., 1993. The geological effects of hurricanes on coral reefs and interpretation of storm  
616 deposits. *Coral Reefs* 12, 203-221. <http://dx.doi.org/10.1007/BF00334480>.

617 Shope, J. B., Storlazzi, C. D. 2019. Assessing Morphologic Controls on Atoll Island Alongshore  
618 Sediment Transport Gradients Due to Future Sea-Level Rise. *Front. Mar. Sci.* 6,  
619 <http://dx.doi.org/10.3389/fmars.2019.00245>.

620 Smithers, S.G., Hoeke, R.K., 2014. Geomorphological impacts of high-latitude storm waves on low-  
621 latitude reef islands. Observations of the December 2008 event on Nukutoa, Takuu, Papua New  
622 Guinea. *Geomorphology* 222: 106–121. <http://dx.doi.org/10.1016/j.geomorph.2014.03.042>.

623 Stoddart, D.R., 1963. Effects of hurricane Hattie on the British Honduras reefs and cays, October 30–  
624 31, 1961. *Atoll Res. Bull.* 95, 1–142.

625 Stoddart, D.R., 1965. Re-survey of hurricane effects on the British Honduras reefs and cays. *Nature*  
626 CCVII, pp. 589–592.

627 Stoddart, D. R., 1969. Post-hurricane changes on the British Honduras reefs and cays: re-survey of  
628 1965. *Atoll Research Bulletin*, 131, 36 p.

629 Stoddart, D. R., 1971. Coral reefs and islands and catastrophic storms. In: Steers, J.A. (Ed.), *Applied*  
630 *Coastal Geomorphology*, Palgrave Macmillan, UK, pp. 155-197.

631 Terorotua, H., 2017. Impacts des événements extrêmes en Polynésie française et contribution à  
632 l'élaboration d'une typologie des îles coralliennes. Rapport de Master 2, La Rochelle University,  
633 STORISK project, 128 p.

634 Thieler, E.R., Himmelstoss, E.A., Zichichi, J.L., Ergul, A., 2009. The Digital Shoreline Analysis  
635 System (DSAS) Version 4.0: an ArcGIS extension for calculating shoreline change. *USGS Open*  
636 *File Report*, pp. 1–79 2008-1278.

637 Tou, J.T., R. C. Gonzalez, 1974. *Pattern Recognition Principles*, Addison-Wesley Publishing  
638 Company, Reading, Massachusetts. <https://doi.org/10.1002/zamm.19770570626>

639 Tuck, M., Kench, P. S., Ford, M.R., Masselink, G., 2019. Physical modelling of the response of reef  
640 islands to sea level rise. *Geology* 47(9), 803-806. <http://dx.doi.org/10.1130/G46362.1>.

641 Tucker C.J., 1979. Red and photographic infrared linear combinations for monitoring vegetation.  
642 Remote Sens. Environ. 8, 127-150.

643 Wadey, M., Brown, S., Nicholls, R. J., Haigh, I., 2017. Coastal flooding in the Maldives: an  
644 assessment of historic events and their implications. Nat. Haz. 89 (1), 131-159.  
645 [http://dx.doi.org/ 10.1007/s11069-017-2957-5](http://dx.doi.org/10.1007/s11069-017-2957-5).

646 Woodroffe, C. D., 1983. The impact of cyclone Isaac on the coast of Tonga. Pacific Science 37(3),  
647 181-210.

648 Yates, M.L., Le Cozannet, G., Garcin, M., Salai, E., Walker, P., 2013. Multi-decadal atoll shoreline  
649 change on Manihi and Manuae, French Polynesia. Journal of Coastal Research 29, 870–892.  
650 <http://dx.doi.org/10.2112/JCOASTRES-D-12-00129.1>.

651

652